

# Probes and magnetospheric plasmas

Erik Engwall

1st November 2004

## 1 Introduction

This report is a summary of a five week literature course, comprising 26 scientific articles, completed in October 2004. The first part covers basic Langmuir probe theory with applications on electric field measurements. In the second part cold magnetospheric plasmas, including observations and possible supply mechanisms, are treated.

## 2 Basic and applied probe theory

Many plasma instruments, e.g. for measurements of electric fields, density and temperature, are based on the Langmuir probe theory [1]. To understand the functioning of these instruments, it is essential to quantify the currents to the probe. This quantification was first carried out by Mott-Smith and Langmuir [1] by using the *orbital motion limited theory* (OML). This theory is not based on plasma physics, but regards a distribution of particles moving in the vacuum field from the probe, thus obtaining trajectories determined only by conservation of energy and angular momentum<sup>1</sup>. This approach can be adopted when the radius of the probe is much smaller than the Debye length. If the probe radius, on the contrary, is much larger than the Debye length, the probe will be efficiently shielded and *sheath limited theory* (SL) must instead be used. In the following, we will only regard OML theory and apply it to spherical probes, noting that it is fully developed also for cylinders.

Mott-Smith and Langmuir [1] treat the currents to a probe in an isotropic plasma. As a starting point, they examine the *random currents*, which are the currents to a probe at zero potential, and then continue with the currents to a charged probe (cf sections 2.1 and 2.2). If the plasma is drifting with respect to the probe, the equations for the currents have to be modified to the form given in section 2.3. In space the photoelectron current often gets important for sunlit probes and adds to the electron and ion currents (cf section 2.4). As described in section 2.5, the currents balance at a certain potential, which is called the *floating potential* of the probe.

### 2.1 Random current

Consider a charged particle with orthonormal velocity components  $u$ ,  $v$  and  $w$  at some distance  $r$  from an *uncharged* spherical probe with radius  $a$ . The component  $u$  gives the radial velocity, counted positive when directed towards the probe, while  $v$  and  $w$

---

<sup>1</sup>Surprisingly enough, we can use the same theories and obtain the same physical relations for currents along an auroral flux tube [2].

are tangential velocity components. In a Maxwellian plasma the distribution function is then given by

$$f(u, v, w) = n \left( \frac{m}{2\pi KT} \right)^{3/2} e^{-\frac{m}{2KT}(u^2+v^2+w^2)}, \quad (1)$$

if we consider a region so far from the probe that absorption by the probe does not change the plasma.

The number of particles per unit volume in the velocity range  $[u, u + du]$ ,  $[v, v + dv]$  and  $[w, w + dw]$  is

$$f(u, v, w) du dv dw = n \left( \frac{m}{2\pi KT} \right)^{3/2} e^{-\frac{m}{2KT}(u^2+v^2+w^2)} du dv dw. \quad (2)$$

If  $\mathbf{p}$  is the resultant of  $v$  and  $w$ , we have that  $p = \sqrt{v^2 + w^2}$ ,  $v = p \cos \Psi$  and  $w = p \sin \Psi$ , where  $\Psi = \arctan(\frac{w}{v})$  ( $p \in [0, \infty[$  and  $\Psi \in [0, 2\pi[$ ). This change of variables yields

$$f(u, v, w) du dv dw = g(u, p, \Psi) \left| \frac{\partial(v, w)}{\partial(p, \Psi)} \right| du dp d\Psi = g(u, p, \Psi) p du dp d\Psi, \quad (3)$$

where

$$g(u, p, \Psi) = n \left( \frac{m}{2\pi KT} \right)^{3/2} e^{-\frac{m}{2KT}(u^2+p^2)}. \quad (4)$$

The current to the probe from the plasma is created by plasma particles hitting the probe. Only particles with positive radial velocities, *i.e.*  $u \in [0, \infty[$ , will reach the probe and contribute to the current. Thus, the particle flux is

$$\Phi = \int_0^{2\pi} \int_0^\infty \int_0^\infty u g(u, p, \Psi) p du dp d\Psi = n \sqrt{\frac{KT}{2\pi m}} \quad (5)$$

The number of particles per second hitting a spherical surface,  $S$ , centered at the probe is then given by  $\eta = S\Phi$ . The current to the probe is obtained by multiplying the above expression by the particle charge,  $q$ , *i.e.*  $I = q\eta$ . At the surface of the probe  $S = 4\pi a^2$ , which gives the final expression for the current:

$$\boxed{I = 4\pi a^2 n q \sqrt{\frac{KT}{2\pi m}} = 2nqa^2 \sqrt{\frac{2\pi KT}{m}} \equiv I_{\text{th}}.} \quad (6)$$

This is the *random current* to a probe in a Maxwellian plasma for the particle species of mass  $m$  and charge  $q$ .

## 2.2 Current to charged probe

In this section, we derive the current to a spherical probe charged to a potential  $V_p$  with respect to the plasma. The potential from a charged object immersed in a plasma will be shielded by charges of opposite sign. A negatively charged object will for example be shielded by a cloud of positive ions. The shielding particles together form a *sheath*, beyond which the potential from the object will not reach. Now consider a particle at the sheath edge,  $s$ , with charge  $q$ , radial velocity  $u$  and tangential velocity components  $v$  and  $w$ . As in the previous section  $v$  and  $w$  are replaced by their resultant  $\mathbf{p}$  and the

same transformation is performed for the distribution function:  $f(u, v, w) du dv dw = g(u, p, \Psi) p du dp d\Psi$ .

The probe current can be obtained through the particle flow to the probe,  $I = qS_a\Phi_a$ , where  $S_a$  is the surface area of the probe and  $\Phi_a$  the particle flux to the probe at its surface ( $r = a$ ). As in the derivation of the random current,  $\Phi(r)$  can be integrated from the distribution function. Inside the sheath, the plasma has been disturbed by the potential from the probe, and the distribution function has to be derived from Liouville's theorem [3], which states that the distribution function along a particle trajectory is constant. If we can trace a particle from the sheath to the probe surface, it is therefore possible to determine the current from the distribution function at  $s$ . Since the plasma is undisturbed outside the sheath, the distribution function at  $s$  is taken to be a common Maxwellian.

The tracing of the particles is performed by considering the principles of conservation of energy and angular momentum. If  $u_a$  and  $q_a$  are the radial and tangential velocity components, respectively, for a particle arriving at the probe surface ( $r = a$ ), we obtain

$$\frac{1}{2}m(u^2 + p^2) = \frac{1}{2}m(u_a^2 + q_a^2) + qV_p \quad (7)$$

$$qs = q_a a, \quad (8)$$

assuming zero potential at infinity.

Combining the equations yields

$$u_a^2 = u^2 - \left(\frac{s^2}{a^2} - 1\right)p^2 - 2\frac{q}{m}V_p \quad (9)$$

$$q_a = \frac{s}{a}p. \quad (10)$$

To reach the probe the particle has to be approaching the probe, *i.e.*  $u > 0$ , since outside the sheath, there is no field that could attract the particle to the probe. Moreover, from a mathematical point of view,  $u_a^2 \geq 0$ . Inserting the last condition into equation (9) leads to the following inequality for  $p$ :

$$p^2 \leq \frac{a^2}{s^2 - a^2} \left(u^2 - 2\frac{q}{m}V_p\right). \quad (11)$$

Let  $q_1 = \sqrt{\frac{a^2}{s^2 - a^2} \left(u^2 - 2\frac{q}{m}V_p\right)}$ , so that the range of  $p$  is  $[0, q_1]$ . Since  $p^2 \geq 0$ , inequality (11) also leads to an additional condition for  $u$ :  $u^2 \geq 2\frac{q}{m}V_p$ , which is automatically satisfied for attractive potentials ( $qV_p < 0$ ). We thus have  $u \geq u_1$ , where  $u_1 = 0$  for attractive potentials and  $u_1 = \sqrt{2\frac{q}{m}V_p}$  for repulsive potentials. At  $r = s$  the flux of particles which will eventually reach the probe and contribute to the current is

$$\begin{aligned} \Phi(s) &= \int_0^{2\pi} \int_{u_1}^{\infty} \int_0^{q_1} u g(u, p, \Psi) p dp du d\Psi = \\ &= n\sqrt{\frac{KT}{2\pi m}} e^{-\frac{m}{2KT}u_1^2} \left[ 1 - \left(\frac{s^2 - a^2}{s^2}\right) \exp\left(\frac{a^2}{s^2 - a^2} \left(\frac{qV_p}{KT} - \frac{m}{2KT}u_1^2\right)\right) \right] \end{aligned} \quad (12)$$

The current to the probe then is

$$\begin{aligned}
I(s) &= qS\Phi(s) \\
&= q4\pi s^2 n \sqrt{\frac{KT}{2\pi m}} e^{-\frac{m}{2KT}u_1^2} \left[ 1 - \left( \frac{s^2 - a^2}{s^2} \right) \exp \left( \frac{a^2}{s^2 - a^2} \left( \frac{qV_p}{KT} - \frac{m}{2KT}u_1^2 \right) \right) \right]
\end{aligned} \tag{13}$$

Letting the sheath expand to infinity, equation (13) takes the form

$$\begin{aligned}
I_\infty &= \lim_{s \rightarrow \infty} I(s) = 4\pi a^2 n q \sqrt{\frac{KT}{2\pi m}} e^{-\frac{m}{2KT}u_1^2} \left( 1 - \frac{qV_p}{KT} + \frac{m}{2KT}u_1^2 \right) = \\
&= I_{th} e^{-\frac{m}{2KT}u_1^2} \left( 1 - \frac{qV_p}{KT} + \frac{m}{2KT}u_1^2 \right)
\end{aligned} \tag{14}$$

In this limiting case there will be no shielding, which means that it corresponds to the current to a probe in vacuum, *i.e.* the OML approximation. For attractive potentials  $u_1 = 0$ , while for repulsive potentials  $u_1 = \sqrt{2\frac{q}{m}V_p}$ . With these values for  $u_1$ , the current to the probe can be expressed as

$$I_\infty = \begin{cases} I_{th} \left( 1 - \frac{qV_p}{KT} \right) & \text{(attractive potentials, } qV_p < 0) \\ I_{th} e^{-\frac{qV_p}{KT}} & \text{(repulsive potentials, } qV_p > 0) \end{cases} \tag{15}$$

where  $I_{th}$  is the random current as shown in equation (6). When  $V_p = 0$ ,  $I_\infty = I_{th}$  as expected.

### 2.3 Probe current in flowing plasma

Medicus ([4], [5]) treats the current to a probe in a flowing plasma. In this case, a particle far away from the probe with velocity  $v$  and impact parameter  $p$  is considered. The particle is outside the sheath surrounding the probe, and thus feels no electrical force. Furthermore, the sheath is assumed to be large compared to the probe so that OML is applicable and all particles that enter the sheath will not reach the probe. This allows *grazing incidence*, which means that also particles with zero radial velocity at the probe surface contribute to the current.<sup>2</sup>

Let  $u$  and  $p$  be the radial and tangential velocity components respectively at the sheath edge ( $r = s$ ). The total velocity is  $v$  ( $v = \sqrt{u^2 + p^2}$ ). The velocities at the probe surface ( $r = a$ ) are denoted by subscript  $a$ .

As before, the constraints are set up by the principles of conservation of energy and angular momentum:

---

<sup>2</sup>This is a simplified treatment compared to Medicus, who also treats the sheath limited case, where any particle entering the sheath will reach the probe.

$$\frac{1}{2}m(u^2 + p^2) = \frac{1}{2}m(u_a^2 + q_a^2) + qV_p \quad (16)$$

$$q_a a = ps = vp \quad (17)$$

In the case of grazing incidence, we have  $u_a = 0$  and the *limiting impact parameter*,  $p_g$ , is then given by

$$p_g^2 = a^2 \left( 1 - 2 \frac{qV_p}{mv^2} \right) \quad (18)$$

For repulsive potentials  $qV_p$  is positive, which means that there is a lower limit on  $v$ , since  $p_g^2 > 0$ . In other words, the velocity of the particle has to be sufficiently high to enable it to overcome the potential barrier and reach the probe. This lower limit is given by

$$v_1 = \sqrt{\frac{2qV_p}{m}}. \quad (19)$$

For accelerating potentials  $p_g^2$  is positive for any  $v \in [0, \infty[$ . All particles with a smaller impact parameter than  $p_g$  will reach the probe. The current to the probe is then given by the flow through the circle with radius  $p_g$ :

$$\begin{aligned} dI &= \pi p_g^2 q n v F(v) dv, \\ &= \pi q n a^2 \left( 1 - 2 \frac{qV_p}{mv^2} \right) v F(v) dv \end{aligned} \quad (20)$$

$$I = \pi q n a^2 \int_{v_1}^{\infty} \left( 1 - 2 \frac{qV_p}{mv^2} \right) v F(v) dv, \quad (21)$$

where  $n$  is the number density,  $F(v)$  the speed distribution<sup>3</sup> and  $v_1$  the minimum speed, which is 0 for accelerating potentials and given by equation (19) for repulsive potentials. For a cold drifting plasma,  $F(v) = \delta(v - v_d)$ , where  $v_d$  is the drift velocity. The current is then

$$\boxed{I = \pi q n a^2 \int_{v_1}^{\infty} \left( 1 - 2 \frac{qV_p}{mv^2} \right) v \delta(v - v_d) dv = \begin{cases} \pi q n a^2 v_d \left( 1 - 2 \frac{qV_p}{mv_d^2} \right) & (v_d \geq v_1) \\ 0 & (v_d < v_1) \end{cases}} \quad (22)$$

The first result holds for all accelerating potentials and for repulsive potentials when the drift velocity is larger than  $v_1$ . It is interesting to compare the equations to a

<sup>3</sup>It may at first seem counterintuitive that we can use a scalar argument  $v$  in the distribution function  $F(v)$ , since the drift clearly produces an anisotropy. However, there is no feedback from the particle distribution on the fields in the OML limit, and therefore the anisotropy is not important for the total current to the probe. To put it simply, the probe doesn't care about what direction the particle arrives from. If plasma effects are important, the sheath becomes anisotropic and the present analysis does not hold.

charged probe in a non-drifting Maxwellian plasma (equation (15)) with equation (22). For the attractive potential, the functional forms are identical, with the drift energy  $\frac{1}{2}mv_d^2$  replacing the thermal energy  $KT$  and  $qnv_d\pi a^2$  replacing the random current  $qn\sqrt{\frac{KT}{2\pi m}}4\pi a^2$ , which is easy to understand from a basic consideration of the situation.

In the random current, the thermal velocity  $\sqrt{\frac{KT}{2\pi m}}$  is replaced by the drift velocity  $v_d$  and  $4\pi a^2$  is replaced by  $\pi a^2$ , since for the flowing plasma a probe at zero potential collects current only from one direction. For repulsive potentials, equation (22) is actually consistent with the limit  $T \rightarrow 0$  of (15).

In the case of a drifting Maxwellian plasma the three dimensional velocity distribution is given by

$$f(v_x, v_y, v_z) = n \left( \frac{m}{2\pi KT} \right)^{\frac{3}{2}} e^{-\frac{m}{2KT} [v_x^2 + v_y^2 + (v_z - v_d)^2]} \quad (23)$$

for a drift in the  $z$ -direction with velocity  $v_d$ . Changing to spherical coordinates we get

$$f(v, \theta, \phi) = n \left( \frac{m}{2\pi KT} \right)^{\frac{3}{2}} e^{-\frac{m}{2KT} [v^2 + v_d^2 - 2vv_d \cos \theta]} \quad (24)$$

The speed distribution is

$$\begin{aligned} F(v) &= \int_0^\pi \int_0^{2\pi} f(v, \theta, \phi) v^2 \sin \theta d\phi d\theta \\ &= 2\sqrt{\frac{m}{2\pi KT}} \frac{v}{v_d} e^{-\frac{m}{2KT} [v^2 + v_d^2]} \sinh \frac{mvv_d}{KT} \end{aligned} \quad (25)$$

Inserting equation (25) into equation (21) yields

$$\begin{aligned} I &= qna^2 \sqrt{\frac{2\pi KT}{m}} \left[ e^{-\frac{m}{2KT} (v_1^2 + v_d^2)} \left( \frac{v_1}{v_d} \sinh \left( \frac{mv_d v_1}{KT} \right) + \cosh \left( \frac{mv_d v_1}{KT} \right) \right) \right. \\ &\quad \left. + \sqrt{\frac{KT}{2mv_d^2}} \left( \frac{mv_d^2}{KT} + 1 - \frac{2qV_p}{KT} \right) E \left( \sqrt{\frac{m}{2KT}} (v_1 - v_d), \sqrt{\frac{m}{2KT}} (v_1 + v_d) \right) \right] \end{aligned} \quad (26)$$

where  $E(a, b) = \int_a^b e^{-y^2} dy$ . In the limit  $v_d \rightarrow 0$ , equation (26) reduces to

$$I = qna^2 \sqrt{\frac{2\pi KT}{m}} e^{-\frac{m}{2KT} v_1^2} \left( \frac{mv_1^2}{KT} - \frac{2qV_p}{KT} + 2 \right). \quad (27)$$

Inserting  $v_1 = 0$  for accelerating potentials and  $v_1 = \sqrt{\frac{2qV_p}{m}}$  for repulsive potentials, we retrieve the classical Langmuir results for a non-drifting plasma (cf. equation (15)). For large drift velocities ( $v_d \rightarrow \infty$ ) both the ion and electron current will approach  $qna^2\pi v_d$  and the total current will thus vanish.

## 2.4 Photoelectron current

For sunlit probes, in addition to plasma ion and electron currents, we have to regard photoelectron currents<sup>4</sup>. In magnetospheric plasmas the photoelectron current will be dominating and the probe will thus be brought to a positive potential. The photoelectron current will depend on the projected area of the probe to the sun,  $A_p$ , the surface properties of the probe, distance to the Sun and the solar spectrum. Because of these different dependences, it is difficult to find a valid theoretical expression for the photoelectron current and it has to be derived from either laboratory experiments [8] or satellite measurements. This implies that there are many different expressions used for the photoelectron current. In this treatment, we adopt the expressions used by Pedersen [9]. One obvious drawback with these expressions is that the time-variability of the solar UV-radiation is neglected. The distance to the Sun is not included either, but this is of less importance for satellites operating in the near-Earth environment.

For *negative potentials* all photoelectrons can escape from the probe and the photoelectron current will be saturated at the constant value  $I_{ph}^0$ :

$$I_{ph} = I_{ph}^0 = A_p j_{ph}^0, \quad V_p < 0 \quad (28)$$

where  $j_{ph}^0$  is the photoelectron current density. From satellite data Pedersen [9] has estimated  $j_{ph}^0$  to around  $80 \mu\text{A}/\text{m}^{-2}$  for a probe operating in space for a long period.

Probes at *positive potentials* will recollect some of the photoelectrons, the more the higher the potential is. The photoelectron current density for a probe at positive potential can be given by the analytic function [9]

$$J_{ph} = 80e^{(-V_p/2)} + 3e^{(-V_p/7.5)} \quad [\mu\text{A}/\text{m}], \quad (29)$$

and the corresponding photoelectron current is given by

$$I_{ph} = A_p J_{ph}, \quad V_p > 0. \quad (30)$$

## 2.5 Current balance

Combining the photoelectron current with the expressions for the electron and ion currents given in sections 2.2 (non-drifting plasma) and 2.3 (drifting plasma), respectively, current-voltage relations for spherical probes can be derived. At equilibrium, the currents will balance each other ( $\sum_n I_n = I_e + I_i + I_{ph} = 0$ ) and the probe will attain its *floating potential*. For sunlit probes operating above Earth's ionosphere, the ion current is negligible and the floating potential is in practice obtained by balancing the current of escaping photoelectrons and impinging plasma electrons. In the magnetosphere, the floating potential is normally a few volts positive [10]. Figure 1 shows the current balance for ambient plasma electrons (blue) and escaping photoelectrons (red) to a probe (radius 4 cm) in a magnetospheric plasma of temperature 10 eV and density  $10 \text{ cm}^{-3}$ . The currents balance each other at approximately 9.3 V positive.

For a probe in shadow, the situation becomes very different. In this case the probe will be at negative potential and if the ion and electron temperatures are equal the current balance equation reduces to

---

<sup>4</sup>In a rigorous treatment other effects, such as secondary electron emission, should also be treated [6], [7], but it is omitted here.

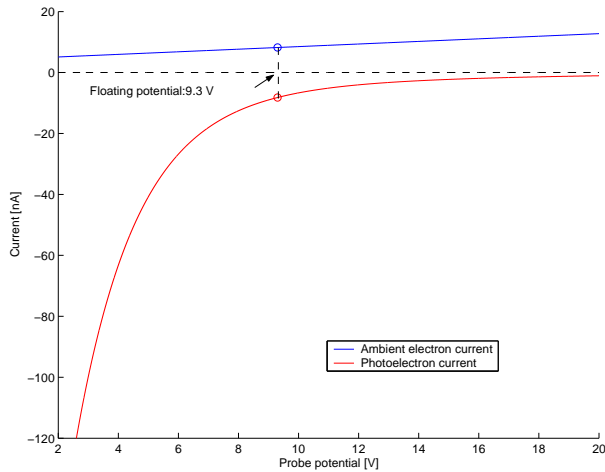


Figure 1: Current balance of impinging plasma electrons and escaping photoelectrons to a probe of radius 4 cm. The temperature of the plasma is 10 eV and the density is  $10 \text{ cm}^{-3}$ . In such a tenuous plasma the ion current is negligible. The floating potential is around 9.3 V.

$$Me^x + x - 1 = 0, \quad (31)$$

where  $x = eV_p/KT_e$  and  $M = \sqrt{m_i/m_e}$ ,  $m_e$  and  $m_i$  being the electron and ion mass respectively. The numerical solution of the equation is  $x = eV_p/KT_e \approx -2.5$ . The negative potential can be explained by the fact that, when the electron and ion temperatures are equal, the electrons will move faster than the ions and thus hit the probe more frequently.

### 3 Electric field measurements with double probes

Langmuir probes have been used for measurements of among other plasma densities, temperatures and electric fields in space since the beginning of the space era, and even earlier in laboratory plasmas. Still, they form the basis in many dominating measurement techniques. To perform these measurements it is important to understand the relations for probe currents treated for spherical probes in section 2. The double probe technique for electric field measurements has been well summarized in [11]. Additional information can be found in [10], [12], [13] and [14].

#### 3.1 Measurement technique

The double-probe instrument uses a conceptually simple technique of measuring the potential difference between two probes in a plasma. A simplified picture of the double-probe electrical system is given in figure 2. For electric field measurements, we are interested in the potential difference  $\Phi_1 - \Phi_2$ . The electric field is obtained by dividing this difference with the probe separation. However, it is only possible to measure the quantity  $U_1 - U_2$ , which equals  $(\Phi_1 - \Phi_2) + (V_1 - V_2)$ , where  $V_1$  and  $V_2$  are the potentials of the probes with respect to the plasma. The double-probe technique is based on the assumption that the coupling between plasma and probe is the same at the two probes, *i.e.*  $V_1 = V_2$ , so that

$$U_1 - U_2 = \Phi_1 - \Phi_2. \quad (32)$$

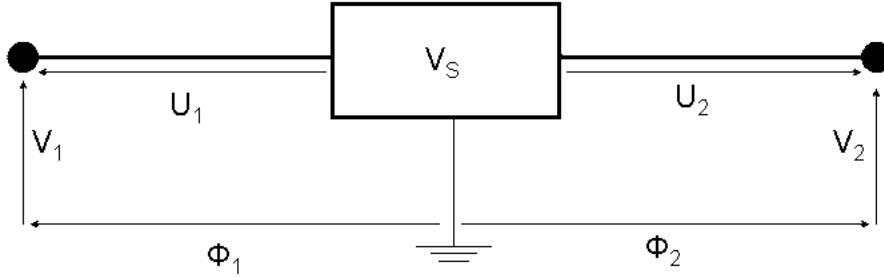


Figure 2: Simplified electrical schema of the double-probe/spacecraft system.  $U_1$  and  $U_2$  are the potentials between spacecraft and probes,  $V_1$  and  $V_2$  the potentials between probes and plasma and  $\Phi_1 - \Phi_2$  the real potential difference in the plasma. The ground point is of course arbitrary.

To achieve this there are some requirements that have to be fulfilled [11], [13]:

1. *Equally shaped probes.* The probes should be equally shaped to avoid that the probe sheaths become different.
2. *Large probe separation.* The separation between the probes should be large to avoid that the probes disturb each other or more likely are affected by the spacecraft. The only practical solution is to mount the probes on wire booms, which are deployed from a spinning spacecraft [11]. A spinning spacecraft leads to other requirements: If we do not want the photoemission to vary with the spin, the probes should be spherical.
3. *Same material and electrical loading.* The probes should be constructed with the same surface material and same electrical loading.

The measured electric field from a double-probe instrument is not the actual electric field in the plasma, since the spacecraft and probes are moving with respect to the plasma [13], [12]. The electric field in the Earth's rest frame,  $\mathbf{E}$ , is obtained from the measured electric field,  $\mathbf{E}'$ , using the formula

$$\mathbf{E} = \mathbf{E}' - \mathbf{v} \times \mathbf{B}, \quad (33)$$

where  $\mathbf{v}$  is the velocity of the satellite in the Earth system and  $\mathbf{B}$  is the Earth's magnetic field. This means that for measurements of the electric field in a frame of reference independent of the spacecraft motion, we also need detailed measurements of  $\mathbf{v}$  and  $\mathbf{B}$ . For a rotating spacecraft with radially deployed probes, it is the spin plane component of the electric field that is measured. To obtain the full electric field vector, it is normally a good assumption to take  $E_{\perp} \gg E_{\parallel}$ , at least for quasi-DC fields. If  $\mathbf{B}$  is not too close to the spin plane, the total field can be constructed from the spin plane component and the relation  $\mathbf{E} \cdot \mathbf{B} = 0$ . One double-probe system on a spinning spacecraft is thus normally sufficient to determine the full electric field vector. However, it will take one spin period, which will prevent measurements of rapidly varying electric fields. If two double-probes are used instead, the total electric field vector can be determined immediately and the only limitation is probe function and telemetry [11].

For measurements in a dense plasma the electron and ion currents are sufficiently high to give a good coupling between probe and plasma. In a tenuous plasma, photoemission is essential for satisfactory probe-plasma coupling, which means that the probes have to be sunlit to function. As can be seen in figure 1, the probes float at a relatively

high potential where the slope of the photoelectron current is small. This means that a small spurious current to one of the probes can result in a large false electric field. It is therefore desirable to bring the probe closer to the plasma potential, where the current-voltage curve is steeper, which can be achieved by applying a bias current from the probe to the spacecraft (cf. figure 3).

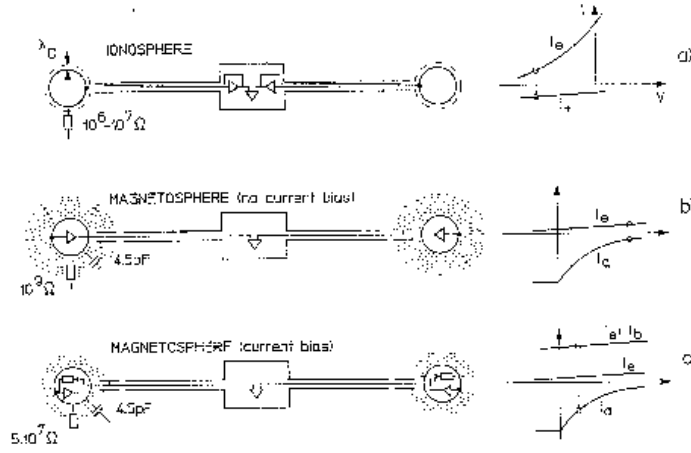


Figure 3: The double-probe instrument in different environments: a) The ionosphere, b) The magnetosphere, c) The magnetosphere with bias current. The bias current brings the probe potential closer to the plasma potential, where small spurious currents will not influence the potential of the probe. Adapted from [11]

The photoelectrons do not only provide the necessary coupling between probe and plasma, but they also solve the severe problems with highly negatively charged satellites and probes [12]. However, the photoemission introduces new errors in the measurement: If the booms are at the same potential as the spacecraft, which is normally the case, the probe furthest away from the Sun will lose more photoelectrons to the booms than the probe closest to the Sun (cf. figure 4). This phenomenon creates a spurious sunward electric field. To prevent this asymmetric current of photoelectrons, the booms are commonly constructed with a negatively biased *guard* close to the probe [10]. The guard will also decrease leakage currents from the spacecraft photoelectrons to the probes and too much influence from the boom potential on the electric field measurement.

The surface of the spacecraft has to be sufficiently conductive to serve as a good reference for the double-probe instrument and the current bias system. In addition, a less conductive surface would create differential charging of the satellite, giving rise to a spurious anti-sunward electric field [10]. For a sufficiently conductive surface, the double-probe instrument also provides two useful by-products[10], [15]:

- *The spacecraft potential.* The spacecraft potential can be determined with an accuracy of  $\pm 1.0$  V from the potential between the probe and the spacecraft. This is useful for interpreting data from particle instruments, and can also be used to derive the plasma density.
- *The plasma density.* The plasma density can be related to the spacecraft po-

tential<sup>5</sup> through the current relations derived in section 2. To get an empirical relation between the plasma density and the spacecraft potential for a specific satellite, the spacecraft potential is compared to the plasma density derived from an on-board density instrument [9], [15], [16]. The advantage of using the spacecraft potential for density measurements is the high sampling frequency and the simplicity to interpret the resulting data. It should be noted that the density alone does not determine the spacecraft potential: the temperature is also a factor, so the temperature has to be assumed to stay within some range for a plasma density-spacecraft potential calibration to be valid.

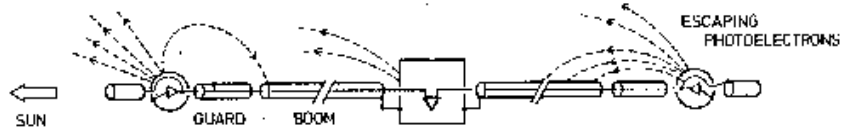


Figure 4: The probe furthest away from the Sun will lose more photoelectrons to the positively charged booms than the probe close to the Sun, which will cause a spurious sunward electric field. This can be prevented by applying a negatively biased guard near the probes.

### 3.2 Complications

Known sources of spurious electric fields influencing measurements by double-probe instruments include:

1. Assymetries of the probes.
2. Coupling between probes and boom tips.
3. Wake effects.
4. Magnetization.
5. Plasma density gradients.

How to prevent effects of the two first causes has already been treated in the previous section. The influence of wakes is covered in [10] and [14]. Comparison with electron drift instruments has shown that formation of a wake behind the spacecraft and booms can severely affect the measurement from double probe instruments. In a tenuous plasma the effects of the wake can be more pronounced than in a dense plasma, since the drift energy of the flowing plasma can be lower than the spacecraft potential and therefore it is not only the spacecraft that constitutes the obstacle for the plasma, but also the potential structure around it. The plasma is in most cases flowing perpendicular to the ambient electric field (in the  $\mathbf{E} \times \mathbf{B}$  direction or parallel to  $\mathbf{B}$ ), which means that the spurious wake electric field will be in this direction, *i.e.* transverse to the real ambient electric field. The wake will thus have more influence on the direction than of the amplitude of the measured transverse electric field. However, the wake induced field along  $\mathbf{B}$  may be many orders of magnitude above any real parallel electric field<sup>6</sup>.

<sup>5</sup>The floating potential of the spacecraft will be very close to that of an unbiased probe.

<sup>6</sup>This is the case in *e.g.* the polar wind, where spurious electric fields due to wakes have been observed [17].

In [18] results from numerical simulations are provided to quantify the wake effects on the Cluster electric field instrument EFW in the polar wind.

Magnetization could also complicate the measurements, when the electron gyroradius is comparable to or smaller than the probe dimensions [13]. In such a case, the probes will mostly collect electrons from a column parallel to the magnetic field. Gradients in the plasma density along the boom direction will cause spurious electric fields, since the basis of the assumption  $V_1 = V_2$  is that the plasma is homogeneous. This error can be reduced by applying an appropriate bias current [19].

A problem with a spinning double-probe system, is that we get the parallel electric field only when the spin axis is perpendicular to  $\mathbf{B}$ . In many cases it would also be interesting to measure parallel electric fields [13], *e.g.* in the auroral acceleration regions.

## 4 Cold magnetospheric plasmas

### 4.1 Mechanisms for supply of cold magnetospheric plasmas

Most of the plasma in the magnetosphere is of ionospheric origin. The ionospheric plasma has low energy, and if it is permitted to escape into the magnetosphere without significant energization, it will remain cold. Ion outflows from the ionosphere can be divided into two types [20]:

1. Ion energization processes
2. Bulk ion outflows

Ion energization processes include for example transversely accelerated ions, ion conics and ion beams. In these processes only a fraction of the ions participate in the outflow. This is in contrast to the bulk ion outflows, where the whole particle distribution is moving. These outflows can thus contribute significantly to the population of cold magnetospheric plasma. The polar wind is an example of bulk ion outflow along magnetic field lines above the polar caps. However, bulk ion outflows occur at all latitudes; *e.g.* outflows of thermal  $O^+$  in the topside auroral ionosphere, and the filling of the plasmasphere are both due to such processes. The bulk ion outflows are strongly dependent on the solar wind properties and the interplanetary magnetic field [21].

Beside bulk ion outflows, the plasmasphere is an important supply of cold plasma. The plasmasphere is directly connected to the ionosphere and is thus filled with cold, dense plasma. At *plasmasphere detachments*, a part of the plasmasphere is ripped away and thus supplies its cold plasma to the magnetosphere.

#### 4.1.1 Polar wind

The polar wind, named after its similarities to the solar wind [22], was theoretically predicted by Axford [22] and Banks and Holzer [23] in 1968 by arguing that the light ions in the ionosphere are too energized to be bound by gravity. The outflow is driven by the gradient in the electron pressure, which makes the electrons drift upward. To maintain charge neutrality, an ambipolar electric field is built up and the ions are dragged upward along with the electrons. Thus, a larger outflow of electrons automatically gives rise to a larger outflow of ions. This is evident *e.g.* in the polar wind on field lines connecting to

the sunlit ionosphere, where the outflows are significantly larger than on the nightside, due to escaping photoenergized atmospheric electrons [20], [24].

#### 4.1.2 Auroral Bulk outflows

As was mentioned above, outflows from the auroral regions are driven by the same processes as the polar wind. However, in these regions the ions are more strongly accelerated, as a result of parallel electric fields and particle-wave interactions [24]. Due to the acceleration, heavy ions are also allowed to escape from the ionosphere and the outflow contains a significant if not dominant fraction of  $O^+$  [20] [24]. The upflowing ions originating in the dayside auroral regions, *the cleft*, will be transported tailward by antisunward convection. This motion of ions forms the *cleft ion fountain* [25].

#### 4.1.3 Plasmasphere detachment

Cold dense plasma is at times observed in the dayside outer magnetosphere and at geosynchronous orbits. This plasma is released from the corotating plasmasphere at high geomagnetic activity and convected westward toward the magnetopause (cf. figure 5), forming the *detached plasmasphere* (or *plasmaspheric tail*). The detachment occurs in connection to increases of the dawn-to-dusk convection electric field in the magnetosphere, which together with the corotation electric field confines the plasma in the plasmasphere [26].

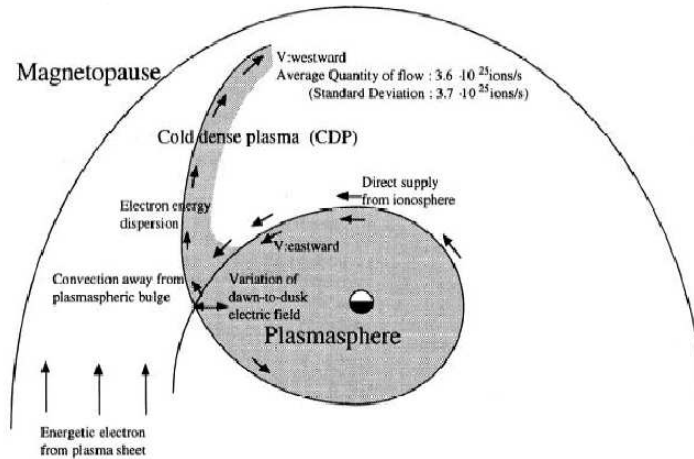


Figure 5: Schematic picture of a plasmaspheric detachment. (Adapted from [26].)

## 4.2 Observations of cold plasmas in the magnetosphere

Observations of cold space plasmas often encounter difficulties. The problems occur especially at low densities, where the spacecraft potential can reach several tens of volts. To reach the detectors mounted on the spacecraft, the ions have to attain a sufficient energy to overcome this potential barrier and reach the spacecraft. This leads to the conclusion that there may exist a much larger fraction of cold plasma in the magnetosphere than has been revealed by previous and current spacecraft missions. In this section, we will investigate some of the observations of cold plasmas in different

regions of the magnetosphere. Figure 6 summarizes where these observations have been carried out.

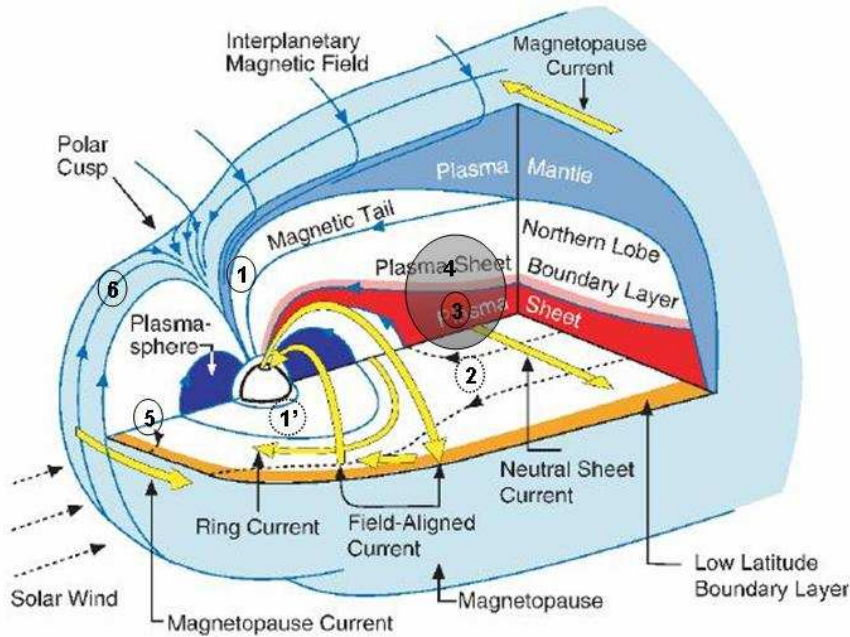


Figure 6: Location of the observations of cold magnetospheric plasma discussed in section 4.2. (Dashed ellipses represent observations in the southern hemisphere.) 1. High altitude polar wind studied by *Su et al.* [27], *Moore et al.* [28] and *Chappell et al.* [29]. 1'. Low altitude polar wind in southern hemisphere by *Su et al.* [27]. 2-4. Cold plasma in the magnetotail observed by *Etcheto and Saint-Marc* [30], *Seki et al.* [31] and *Sauvaud et al.* [32]. 5-6. Studies of cold plasma populations in the dayside magnetosphere by *Chen and Moore* [33] and *Sauvaud et al.* [34]. (Original figure adapted from [35].)

#### 4.2.1 Polar regions

Measurements of the polar wind have indeed been problematic, due to its tenuous cold plasma. The first direct measurements of the polar wind was achieved in the 1970's by Explorer 31, which found  $H^+$  outflows between 500 and 3000 km with velocities up to 10 km/s. ISIS 2 confirmed the outflow of  $H^+$ , but also found evidence for outflows of  $He^+$  at 1400 km. Both these measurements were carried out at low altitude, where the densities were high and thus the spacecraft potentials were low. Contributions to the understanding of the polar wind have also been made by DE 1. The current knowledge of the polar wind can mainly be attributed to studies by Akebono [36], [37] and Polar [27], [28], [29]. The Polar spacecraft was launched in 1996 into a polar ecliptical orbit with  $9 R_E$  apogee (northern hemisphere) and  $1.8 R_E$  perigee (southern hemisphere). Polar carries the ion detector TIDE (Thermal Ion Dynamics Experiment), which operates with good resolution in the 0.3-450 eV energy range. Together with the Plasma Source Instrument (PSI), which reduces the spacecraft potential to approximately +2V by creating a plasma cloud around the spacecraft, TIDE is able to measure low-energy ions. These two instruments have shed new light on the dynamism and composition of the polar wind at different altitudes.

*Su et al.* [27] used Polar data to study the polar wind at two different altitudes:  $8 R_E$  (apogee, northern hemisphere) and 5000 km (perigee, southern hemisphere). Figure

7 illustrates the observed characteristics of the high altitude polar wind, which was first confirmed to exist by Polar [28]. These polar wind observations reveals a faster, hotter and more rich in  $O^+$  plasma than predicted by thermal outflow theories. The discrepancy between theory and observations is probably primarily a result of neglecting energy input in the topside auroral ionosphere [24]. At 5000 km, the  $H^+$  are outflowing, but the mean velocity of  $O^+$  is directed downward (cf figure 8). The high altitude  $O^+$  can thus not originate from the polar cap proper, but are transported into the polar cap from the dayside auroral zone by the cleft ion fountain (cf. section 4.1.2). Parts of the ion distribution are again trapped in the Earth's gravity field over the polar caps and flow downward.

The polar wind survey by *Su et al.* revealed the following parameters of the polar wind:

**Density** At 5000 km the dominant ion species is  $O^+$  ( $n_{O^+} \approx 8\text{cm}^{-3}$ ,  $n_{H^+} \approx 2\text{cm}^{-3}$ ), whereas at  $8 R_E$  the plasma is totally dominated by  $H^+$  ( $n_{O^+} \approx 0.05\text{cm}^{-3}$ ,  $n_{H^+} \approx 0.3\text{cm}^{-3}$ ).  $He^+$  only constitutes a small fraction of the total number of ions at both altitudes.

**Flow speeds** The polar wind exhibits a wide variation in flow speeds with altitude:

- *5000 km:* The  $H^+$  ions are supersonic and upflowing with an average velocity of 15 km/s, while the  $O^+$  ions are subsonic and moving towards the earth with an average velocity of 1 km/s.
- *8  $R_E$ :* Both  $H^+$  and  $O^+$  are supersonic and flowing upwards. The average velocity for  $H^+$  is 45 km/s and for  $O^+$  27 km/s.

These results are somewhat in contradiction with thermal outflow theories, but are consistent with the cleft ion fountain mechanism.

**Temperature** At 5000 km the perpendicular temperatures are higher than the parallel temperatures for both ion species, which may indicate perpendicular heating by wave-particle interactions. At  $8 R_E$  the parallel temperatures are higher than the perpendicular temperature, probably as a result of adiabatic conversion of perpendicular to parallel energy during outward motion along magnetic field lines. The temperature of  $O^+$  is higher than of  $H^+$  at both altitudes. In general, the temperatures are higher than predicted by thermal theories.

The outflowing polar wind contributes significantly to the magnetospheric plasma. Using TIDE/PSI observations together with a particle trajectory code *Chappell et al.* [29] showed that low energy polar wind ions (less than 10 eV) travel out through the lobes into the magnetotail to supply the plasma sheet (cf. figure 9). Moving into the plasma sheet the ions get heated fast to typical plasma sheet energies. (This result was obtained from the particle simulations, which only included the magnetic field of the neutral sheet and the dawn-to-dusk convection electric field, but not wave-particle interactions.) As depicted in figure 10, the energy of the outflowing ions changes also in the polar region itself. These changes occur mainly in the auroral regions, where parallel electric fields and wave-particle interactions are frequent. The accelerated ion outflow, such as ion beams, is referred to as the 'nonclassical' polar wind. The 'classical' polar wind is the normal ambipolar outflow (cf section 4.1.1) [38].

#### 4.2.2 Magnetotail

As described in the previous section, outflowing cold ions from the polar regions are transported to the lobes and into the magnetotail. Such cold ions have been observed

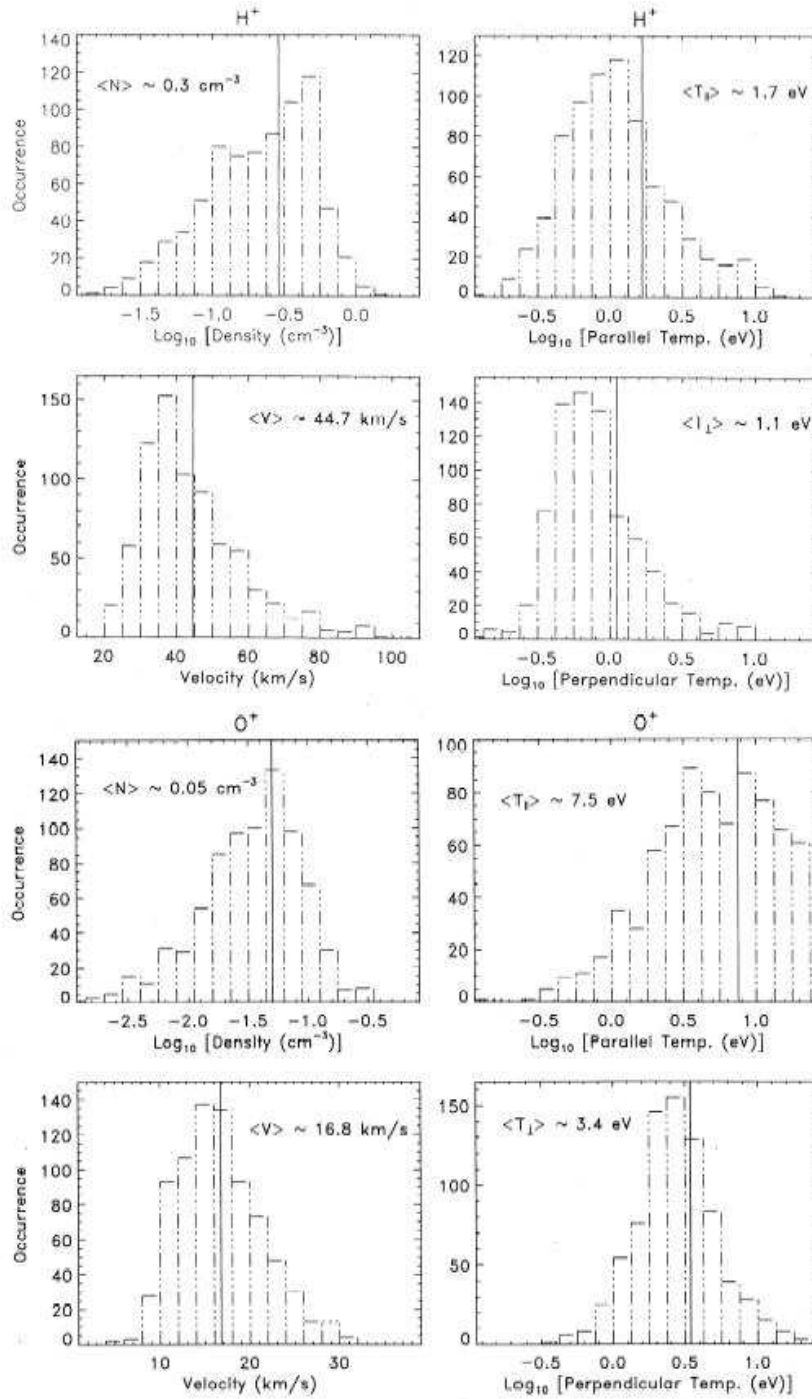


Figure 7: Observations of the high altitude polar wind, for  $H^+$  (higher panels) and  $O^+$  (lower panels). (Adapted from [27].)

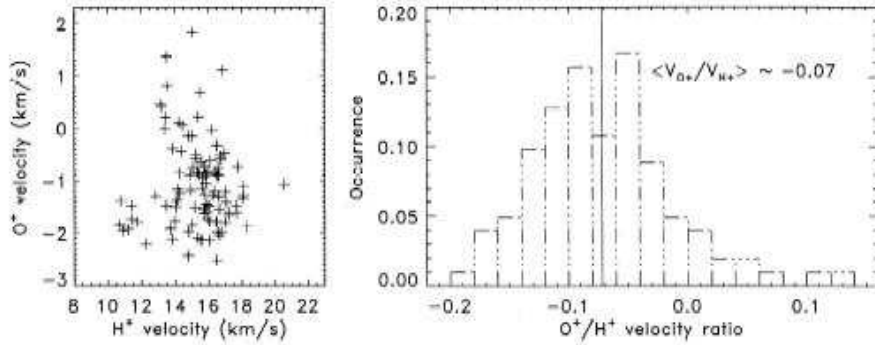


Figure 8: Polar wind flow velocities for  $H^+$  and  $O^+$  at 5000 km, where  $O^+$  is on average downward moving. (Adapted from [27].)

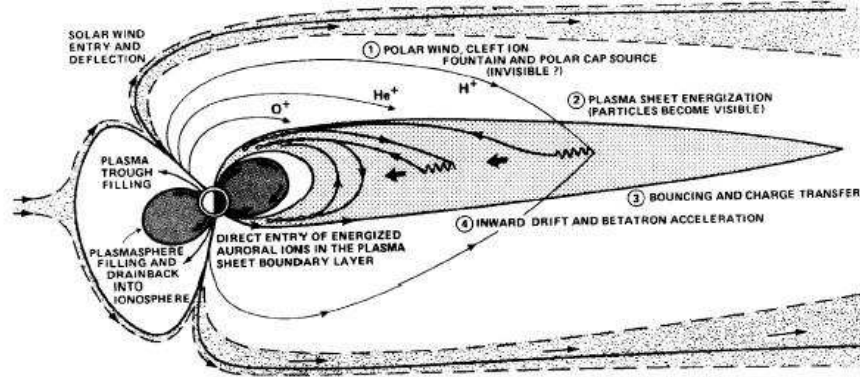


Figure 9: The polar wind supplies plasma to the magnetosphere. Cold polar wind ions drift in the lobes into the plasma sheet, where they get energized. (Adapted from [29].)

in the lobes, the plasma sheet boundary layer (PSBL) and the plasma sheet [30], [31], [32].

*Seki et al.* [31] reported cold ions in the plasma sheet, which were exempted from heating. The observations were made by the GEOTAIL spacecraft at a position of  $9 R_E$  from the Earth. At the time of observation the spacecraft was in the shadow of the Earth, yielding a negative spacecraft potential as a result of prohibited photoelectron emission. The negative spacecraft potential allowed detection of all distributions of ions, regardless of temperature. The authors suggest that the cold ions may not have passed through the boundary heating region adjacent to the plasmasphere (the PSBL), but have directly flown out from the ionosphere. However, the gradual filling of a magnetic flux tube that has already passed the heating region would take several hours, which is much longer than the transport of the flux tube predicted by ordinary magnetic convection theory. If this interpretation is correct, ionospheric outflow fluxes predict that the conventional ideas of magnetospheric convection have to be reformulated.

In the PSBL *Etcheto and Saint-Marc* [30] found anomalously high plasma densities (around  $5 \text{ cm}^{-3}$ ) and low perpendicular energies (less than 30 eV) using several experiments on board the two ISEE spacecraft. The origin of the cold and dense plasma was not possible to deduce in this study, but the authors give two possible explanations:

1. *Detachments from the plasmasphere:* Cold plasmaspheric detachments are convected into the nightside magnetotail.

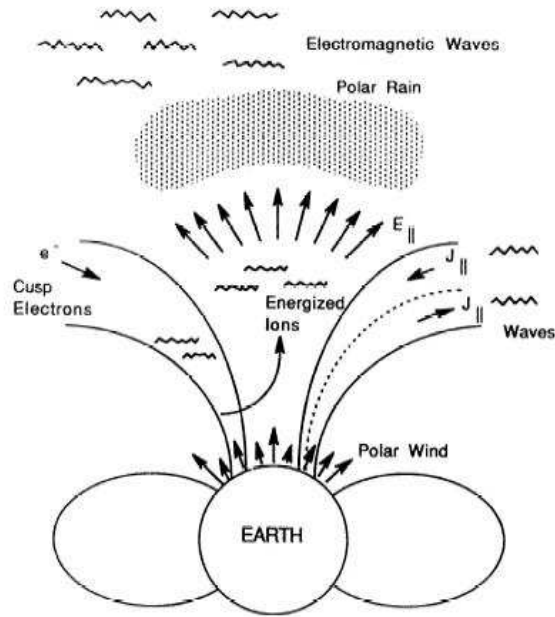


Figure 10: Schematic picture of different acceleration processes that can affect the polar wind. (Adapted from [39].)

2. *Outflowing ions from polar regions*: High density plasma in the polar ionosphere supplies the PSBL.

*Sauvaud et al.* [32] have presented case studies of cold ions in the lobes, the plasma sheet and PSBL using the Cluster ion spectrometers (CIS). These ions have only been detected for high drift velocities, when the drift energy is high enough to overcome the spacecraft potential barrier. The study confirms the idea of transport of ionospheric ions into the magnetotail and show in particular that ions are massively injected from the nightside ionosphere into the tail during storms and substorms. One single injection can even account for over 80% of the plasma sheet  $O^+$  population. Furthermore, the observations of a cold proton population inside the PSBL during quiet times preceding a substorm was reported. The cold ions are accelerated to several hundreds km/s as a result of fast flows in the PSBL<sup>7</sup>, which allows to measure the density of this population precisely. The density of the cold population of around  $0.1 \text{ cm}^{-3}$  is almost comparable to the density of the hot plasma sheet ions, which reaches a maximum of  $0.25 \text{ cm}^{-3}$  in this study.

#### 4.2.3 Dayside magnetosphere

Plasmaspheric detachments can expell large amounts of cold dense plasma into the dayside magnetosphere, which has been observed by many spacecraft<sup>8</sup>. This plasmaspheric plasma contributes to both microscale and macroscale physical processes. Recent observations with Polar [33] have revealed a large number of plasmaspheric ions flowing with high velocity towards the subsolar magnetopause. These fast flows seem to occur

<sup>7</sup>The occurrence of such fast flows in the PSBL can create Alfvén perturbations in the lobe, which have also been observed in the present study by *Sauvaud et al.* [32]. The flows could also trigger Kelvin-Helmholtz instabilities.

<sup>8</sup>e.g. Ogo 4, 5, and 6, Ariel 3, ATS and LANL geostationary satellites ([33], and references therein).

predominantly at southward IMF, which may suggest that they are related to the process of reconnection at the dayside magnetopause: the plasmaspheric detachment flows to fill the low density reconnection region, bringing its frozen in flux tubes towards the approaching solar wind, thus contributing to new reconnection processes.

Cold ions have also been observed by Cluster in the upper dayside magnetosphere adjacent to the magnetopause [34]. These ions became visible to CIS only when they were accelerated by intermittent motion of the magnetosphere. However, they were shown to exist at all times by simultaneous observations with the WHISPER<sup>9</sup> experiment. The density of this cold ion population was found to be as high as  $1 \text{ cm}^{-3}$ , which is much higher than the surrounding local density of ions.

---

<sup>9</sup>Whisper of High frequency and Sounder for Probing Electron density by Relaxation (cf. e.g. [40]).

## References

- [1] H.M. Mott-Smith and I. Langmuir. The theory of collectors in gaseous discharges. *Physical Review*, 28:727–763, 1926.
- [2] R. Boström. Kinetic and space charge control of current flow and voltage drops along magnetic flux tubes: Kinetic effects. *Journal of Geophysical Research*, 108, 2003. doi: 10.1029/2002JA009295.
- [3] H. Goldstein, C. Poole, and J. Safko. *Classical Mechanics*. Addison Wesley, San Fransisco, 3rd edition, 2002.
- [4] G. Medicus. Theory of electron collection of spherical probes. *Journal of Applied Physics*, 32:2512–2520, 1961.
- [5] G. Medicus. Spherical Langmuir probe in "drifting" and "accelerated" Maxwellian distribution. *Journal of Applied Physics*, 33:3094–3100, 1962.
- [6] H. B. Garrett. The charging of spacecraft surfaces. *Reviews of Geophysics and Space Physics*, 19(4):577–616, 1981.
- [7] A. I. Eriksson, L. Wedin, J.-E. Wahlund, and B. Holback. Analysis of Freja charging events: Modelling of Freja observations by spacecraft charging codes. IRF Scientific Report 252, Swedish Institute of Space Physics, 1999.
- [8] R. J. L. Grard. Properties of the satellite photoelectron sheath derived from photoemission laboratory measurements. *Journal of Geophysical Research*, 78:2885–2906, 1973.
- [9] A. Pedersen. Solar wind and magnetosphere plasma diagnostics by spacecraft electrostatic potential measurements. *Annales Geophysicae*, 13:118–121, 1995.
- [10] A. Pedersen, C. A. Cattell, C.-G. Fälthammar, V. Formisano, P.-A. Lindqvist, F. Mozer, and R. Torbert. Quasistatic electric field measurements with spherical double probes on the GEOS and ISEE satellites. *Space Science Reviews*, 37:269–312, 1984.
- [11] A. Pedersen, F. Mozer, and G. Gustafsson. Electric field measurements in a tenuous plasma with spherical double probes. In *Measurement Techniques in Space Plasmas: Fields*, Geophysical Monograph 103, pages 1–12. American Geophysical Union, 1998.
- [12] F. S. Mozer. Analyses of techniques for measuring DC and AC electric fields in the magnetosphere. *Space Science Reviews*, 14:272–313, 1973.
- [13] U. Fahlson. Theory of electric field measurements conducted in the magnetosphere with electric probes. *Space Science Reviews*, 7:238–262, 1967.
- [14] O. H. Bauer, R. Grard, G. Haerendel, and A. Pedersen. Influence of wake and photoemission on electric field measurements with a double probe on GEOS-2. In *Spacecraft/Plasma Interactions and their Influence on Field and Particle Measurements*, ESA SP-198, pages 51–56, 1983.
- [15] A. Pedersen, P. Décréau, P. Escoubet, G. Gustafsson, H. Laakso, P.-A. Lindqvist, B. Lybekk, F. Mozer, and A. Vaivads. Four-point high time resolution information on electron densities by the electric field experiments (EFW) on Cluster. *Annales Geophysicae*, 19:1483–1489, 2001.

- [16] C. P. Escoubet, A. Pedersen, R. Schmidt, and P. A. Lindqvist. Density in the magnetosphere inferred from ISEE 1 spacecraft potential. *Journal of Geophysical Research*, 102:17595–17609, 1997.
- [17] A. Eriksson, M. André, B. Klecker, H. Laakso, P.-A. Lindqvist, F. Mozer, G. Paschmann, A. Pedersen, J. Quinn, R. Torbert, K. Torkar, and H. Vaith. Cluster comparison of the double-probe and electron drift techniques for measuring the electric field. Submitted to *Annales Geophysicae*, June 2004.
- [18] E. Engwall. Numerical studies of spacecraft-plasma interaction: Simulations of wake effects on the Cluster electric field instruments EFW. IRF Scientific Report 284, Swedish Institute of Space Physics, 2004.
- [19] H. Laakso, T. L. Aggson, and R. Pfaff Jr. Plasma gradient effects on double probe measurements in the magnetosphere. *Annales Geophysicae*, 13:130–146, 1995.
- [20] A. W. Yau and M. André. Sources of ion outflow in the high latitude ionosphere. *Space Science Reviews*, 80:1–25, 1997.
- [21] C. M. Cully, E. F. Donovan, A. W. Yau, and G. G. Arkos. Akebono/suprathermal mass spectrometer observations of low-energy ion outflow: Dependence on magnetic activity and solar wind conditions. *Journal of Geophysical Research*, 108, doi: 10.1029/2001JA009200 2003.
- [22] W. I. Axford. The polar wind and the terrestrial helium budget. *Journal of Geophysical Research*, 73:6855–6859, 1968.
- [23] P. M. Banks and T. E. Holzer. The polar wind. *Journal of Geophysical Research*, 73(21):6846–6854, 1968.
- [24] T. E. Moore, M. O. Chandler, C. R. Chappell, R. H. Comfort, P. D. Craven, D. C. Delcourt, H. A. Elliot, B. L. Giles, J. L. Horwitz, C. J. Pollock, and Y.-J. Su. Polar/TIDE results on polar ion outflows. In *Sun-Earth Plasma Connections*, Geophysical Monograph 109, pages 87–101. American Geophysical Union, 1999.
- [25] M. Lockwood, M. O. Chandler, J. L. Horwitz, J. H. Waite Jr., T. E. Moore, and C. R. Chappell. The cleft ion fountain. *Journal of Geophysical Research*, 90:9736–9748, 1985.
- [26] H. Matsui, T. Mukai, S. Ohtani, K. Hayashi, R. C. Elphic, M. F. Thomsen, and H. Matsumoto. Cold dense plasma in the outer magnetosphere. *Journal of Geophysical Research*, 104:25077–25095, 1999.
- [27] Y.-J. Su, J.L. Horwitz, T.E. Moore, B.L. Giles, M.O. Chandler, P.D. Craven, M. Hirahara, and C.J. Pollock. Polar wind survey with the Thermal Ion Dynamics Experiment/Plasma Source Instrument suite aboard POLAR. *Journal of Geophysical Research*, 103:29305–29337, 1998.
- [28] T. E. Moore, C. R. Chappell, M. O. Chandler, P. D. Craven, B. L. Giles, C. J. Pollock, J. L. Burch, D. T. Young, J. H. Waite Jr., J. E. Nordholt, M. F. Thomsen, D. J. McComas, J. J. Berthelier, W. S. Williamson, R. Robson, and F. S. Mozer. High-altitude observations of the polar wind. *Science*, 277:349–351, 1997.
- [29] C. R. Chappell B. L. Gilses, T. E. Moore, D. C. Delcourt, P. D. Craven, and M. O. Chandler. The adequacy of the ionospheric source in supplying magnetospheric plasmas. *Journal of Atmospheric and Solar-Terrestrial Physics*, 62:421–436, 2000.

- [30] J. Etcheto and A. Saint-Marc. Anomalously high plasma densities in the plasma sheet boundary layer. *Journal of Geophysical Research*, 90:5338–5344, 1985.
- [31] K. Seki, M. Hirahara, M. Hoshino, R. C. Elphic, T. Terasawa, Y. Saito, T. Mukai, H. Hayakawa, H. Kojima, and H. Matsumoto. Cold ions in the hot plasma sheet of Earth’s magnetotail. *Nature*, 422:589–591, 2003.
- [32] J.-A. Sauvaud, P. Louarn, G. Fruit, H. Stenuit, C. Vallat, J. Dandouras, H. Rème, M. André, A. Balogh, M. Dunlop, L. Kistler, E. Möbius, C. Mouikis, B. Klecker, G. K. Parks, J. McFadden, C. Carlson, F. Marcucci, G. Pallochia, R. Lundin, A. Korth, and M. McCarthy. Case studies of the dynamics of ionospheric ions in the Earth’s magnetotail. *Journal of Geophysical Research*, 109, doi: 10.1029/2003JA009996 2004.
- [33] S.-H. Chen and T. E. Moore. Dayside flow bursts in the Earth’s outer magnetosphere. *Journal of Geophysical Research*, 109, doi: 10.1029/2003JA010007 2004.
- [34] J.-A. Sauvaud, R. Lundin, H. Rème, J. McFadden, C. Carlson, G. Parks, E. Möbius, L. M. Kistler, B. Klecker, E. Amata, A. M. DeLellis, V. Formisano, J. M. Bosqued, I. Dandouras, P. Décréau, M. Dunlop, L. Eliasson, A. Korth, B. Lavraud, and M. McCarthy. Intermittent thermal plasma acceleration linked to sporadic motions of the magnetopause, first Cluster results. *Annales Geophysicae*, 19:1523–1532, 2001.
- [35] M. G. Kivelson and C. T. Russell. *Introduction to Space Physics*. Cambridge University Press, Cambridge, 1995.
- [36] T. Abe, B. A. Whalen, A. W. Yau, R. E. Horita, S. Watanabe, and E. Sagawa. EXOS-D (Akebono) SMS observations of the polar wind. *Journal of Geophysical Research*, 98:11191–11203, 1993.
- [37] T. Abe, S. Watanabe, B. A. Whalen, A. W. Yau, and E. Sagawa. Observations of polar wind and thermal ion outflow by Akebono/SMS. *Journal of Geomagnetism and Geoelectricity*, 48:319–325, 1996.
- [38] R. W. Schunk. Ionospheric outflow. In *Sun-Earth Plasma Connections*, Geophysical Monograph 109, pages 195–206. American Geophysical Union, 1999.
- [39] R. W. Schunk and J. J. Sojka. Global ionosphere-polar wind system during changing magnetic activity. *Journal of Geophysical Research*, 102:11625–11651, 1997.
- [40] P. M. E. Décréau, P. Ferreau, V. Krasnoselskikh, E. Le Guirriec, M. Lévêque, Ph. Martin, F. X. Sené, O. Randriamboarison, J. L. Rauch, H. C. Séran, J. G. Trotignon, P. Canu, N. Cornilleau, H. de Féraudy, H. Alleyne, K. Yearby, P. B. Mögensen, G. Gustafsson, M. André, D. C. Gurnett, F. Darrouzet, J. Lemaire, C. C. Harvey, P. Travnicek, and Whisper experimenters. Early results from the WHISPER instrument on Cluster: an overview. *Annales Geophysicae*, 19:1241–1258, 2001.